Statistics of mixing in three-dimensional Rayleigh–Taylor turbulence at low Atwood number and Prandtl number one

G. Boffetta,[1] A. Mazzino,[2] S. Musacchio,[3] and L. Vozella[2]
[1]*Dipartimento di Fisica Generale and INFN, Università di Torino, via P. Giuria 1, 10125 Torino, Italy and CNR-ISAC, Sezione di Torino, corso Fiume 4, 10133 Torino, Italy*
[2]*Dipartimento di Fisica, INFN and CNISM, Università di Genova, via Dodecaneso 33, 16146 Genova, Italy*
[3]*CNRS UMR 6621, Lab. J. A. Dieudonnné, Université de Nice Sophia-Antipolis, Parc Valrose, 06108 Nice Cedex 02, France*

(Received 14 October 2009; accepted 6 February 2010; published online 31 March 2010)

Three-dimensional miscible Rayleigh–Taylor (RT) turbulence at small Atwood number and at Prandtl number one is investigated by means of high resolution direct numerical simulations of the Boussinesq equations. RT turbulence is a paradigmatic time-dependent turbulent system in which the integral scale grows in time following the evolution of the mixing region. In order to fully characterize the statistical properties of the flow, both temporal and spatial behaviors of relevant statistical indicators have been analyzed. Scaling of both global quantities (e.g., Rayleigh, Nusselt, and Reynolds numbers) and scale dependent observables built in terms of velocity and temperature fluctuations are considered. We extend the mean-field analysis for velocity and temperature fluctuations to take into account intermittency, both in time and space domains. We show that the resulting scaling exponents are compatible with that of the classical Navier–Stokes turbulence advecting a passive scalar at comparable Reynolds number. Our results support the scenario of universality of turbulence with respect to both the injection mechanism and the geometry of the flow. © *2010 American Institute of Physics*. [doi:10.1063/1.3371712]

I. INTRODUCTION

The Rayleigh–Taylor (RT) instability is a well-known fluid-mixing mechanism originating at the interface between light fluids accelerated into a heavy fluid. It was first described by Rayleigh[1] for incompressible fluid under gravity and later generalized to all accelerated fluid by Taylor.[2]

RT instability plays a crucial role in many fields of science and technology. In particular, in gravitational fusion it has been recognized as the dominant acceleration mechanism for thermonuclear reactions in type-Ia supernovae.[3,4] The efficiency of inertial confinement fusion depends dramatically on the ability to suppress RT instability on the interface between the fuel and the pusher shell.[5,6]

In a late stage, RT instability develops into the so-called RT turbulence in which a layer of mixed fluid grows in time, increasing the kinetic energy of the flow at the expenses of the potential energy. This process finds applications in many fields, e.g., atmospheric and oceanic buoyancy driven mixing. Despite the great importance and long history of RT turbulence, a consistent phenomenological theory has been proposed only recently.[7] In three dimensions, this theory predicts a Kolmogorov-like scenario, with a quasistationary energy cascade in the mixing layer. The prediction is based on the Kolmogorov–Obukhov picture of turbulence in which density fluctuations are transported passively in the cascade and kinetic-energy flux is scale independent.[8] Quasistationarity is a consequence of the Kolmogorov scaling of characteristic times associated to turbulent eddies: Large scales grow driven from potential energy, while small-scale structures, fed by the turbulent cascade, follow adiabatically large-scale growth. These theoretical predictions have been partially confirmed by recent numerical studies.[3,9–11] Other alternative phenomenological approaches (see, e.g., Ref. 12) does not necessarily lead to the Kolmogorov scaling for the energy spectra.

In this paper we carry out an analysis of the scaling behavior of relevant observables with the aim of deepening our previous investigation.[11] Indeed, our aim is to make a careful investigation of the time evolution of global observables and of spatial/temporal scaling and intermittency. Moreover we push the analogy of RT turbulence with the usual Navier–Stokes (NS) turbulence much further. We show that small-scale velocity and temperature fluctuations develop intermittent distributions with structure function scaling exponents consistent with NS turbulence advecting a passive scalar.

This paper is organized as follows. In Sec. II we formulate the problem and outline the phenomenology. After providing a description of the numerical setup in Sec. III, we describe our results in Secs. IV and V. Section IV is devoted to the investigation of the temporal evolution of global quantities. In Sec. V we focus on the statistics at small scales. Finally, the conclusions are provided by summarizing the main results.

II. EQUATION OF MOTION AND PHENOMENOLOGY

We consider the three-dimensional (3D) Boussinesq equations for an incompressible velocity field ($\nabla \cdot \mathbf{v}=0$),

$$\partial_t \mathbf{v} + \mathbf{v} \cdot \nabla \mathbf{v} = -\nabla p + \nu \triangle \mathbf{v} - \beta \mathbf{g} T, \tag{1}$$

TABLE I. Parameters of the simulations: N_x, N_y, and N_z spatial resolutions, ν viscosity, κ thermal diffusivity, and $R_\lambda = v_{\rm rms}^2\sqrt{15/(\nu\epsilon)}$ Reynolds number evaluated at the end of the simulation. All dimensional quantities are made dimensionless using the vertical box size L_z, the characteristic time $\tau=(L_z/Ag)^{1/2}$, and the temperature jump θ_0 as reference units.

Label	$N_x=N_y$	N_z	$\nu=\kappa$ $(\times 10^{-6})$	R_λ
A	256	1024	9.5	103
B	512	2048	4.8	196
C	1024	1024	3.2	122

$$\partial_t T + \mathbf{v}\cdot\nabla T = \kappa\Delta T, \tag{2}$$

with $T(\mathbf{x},t)$ being the temperature field, proportional to the density via the thermal expansion coefficient β as $\rho=\rho_0\times[1-\beta(T-T_0)]$ (ρ_0 and T_0 are reference values), ν is the kinematic viscosity, κ is the molecular diffusivity, and $\mathbf{g}=(0,0,-g)$ is the gravitational acceleration.

At time $t=0$ the system is at rest with cooler (heavier, density ρ_2) fluid placed above the hotter (lighter, density ρ_1) one. This corresponds to $\mathbf{v}(\mathbf{x},0)=(0,0,0)$ and to a step function for the initial temperature profile: $T(\mathbf{x},0)=-(\theta_0/2)\mathrm{sgn}(z)$, where θ_0 is the temperature jump which fixes the Atwood number $A=(\rho_2-\rho_1)/(\rho_2+\rho_2)=(1/2)\beta\theta_0$. The development of the instability leads to a mixing zone of width h that starts from the plane $z=0$ and is dimensionally expected to grow in time according to $h(t)=\alpha Agt^2$ (where α is a dimensionless constant to be determined), which implies the relation $v_{\rm rms}\simeq Agt$ for typical velocity fluctuations (root mean square velocity) inside the mixing zone.

The convective state is characterized by the turbulent heat flux and energy transfer as a function of mean temperature gradient. In terms of dimensionless variables, these quantities are represented respectively by the Nusselt number $\mathrm{Nu}=1+\langle wT\rangle h/(\kappa\theta_0)$ (w being the vertical velocity) and the Reynolds number $\mathrm{Re}=v_{\rm rms}h/\nu$ as a function of the Rayleigh number $\mathrm{Ra}=\beta g\theta_0 h^3/(\nu\kappa)$ and the Prandtl number $\mathrm{Pr}=\nu/\kappa$. Here and in the following $\langle\cdots\rangle$ denotes spatial average inside the turbulent mixing zone, while the overbar indicates the average over horizontal planes at fixed z.

One of the most important problems in thermal convection is to find the functional relation between the convective state characterized by Nu and Re and the parameter space defined by Ra and Pr.[13] The existence of an asymptotic regime at high Ra, with a simple power law dependence $\mathrm{Nu}\sim\mathrm{Ra}^\xi$ and $\mathrm{Re}\sim\mathrm{Ra}^\gamma$, is still controversial in the case of the Rayleigh–Bénard convection, despite the number of experiments at very large Ra. Most of the experiments have reported an exponent $\xi\simeq 0.3$ (Refs. 14 and 15) of a more complex behavior[16,17] partially described by a phenomenological theory.[18] However, many years ago, Kraichnan[19] predicted an asymptotic exponent $\xi=1/2$ (with logarithmic corrections) associated to the now called "ultimate state of thermal convection," while exponents $\xi>1/2$ are excluded by a rigorous upper bound $\mathrm{Nu}\le(1/6)\mathrm{Ra}^{1/2}-1$.[20] The ultimate state regime is expected to hold when thermal and kinetic boundary layers become irrelevant, and indeed has been observed in numerical simulations of thermal convection at moderate Ra when boundaries are removed,[21] while no indication of ultimate state regime has been observed in Rayleigh–Bénard experiments.[14]

The ultimate state exponent is formally derived from kinetic energy and temperature balance equations.[18] In the present context of RT turbulence they can more easily be obtained from the temporal scaling of h and $v_{\rm rms}$. Assuming that $\langle wT\rangle\sim v_{\rm rms}\theta_0$, using the above definitions one estimates,

$$\mathrm{Ra}\simeq(Ag)^4t^6/(\nu\kappa),\quad \mathrm{Re}\simeq(Ag)^2t^3/\nu,\quad \text{and}\quad \mathrm{Nu}\simeq(Ag)^2t^3/\kappa, \tag{3}$$

from which

$$\mathrm{Nu}\sim\mathrm{Pr}^{1/2}\mathrm{Ra}^{1/2}\quad\text{and}\quad\mathrm{Re}\sim\mathrm{Pr}^{-1/2}\mathrm{Ra}^{1/2}. \tag{4}$$

For what concerns the small-scale statistics inside the mixing zone, the phenomenological theory[7] predicts for the 3D case an adiabatic Kolmogorov–Obukhov scenario with a time-dependent kinetic-energy flux $\epsilon\simeq v_{\rm rms}^3/h\simeq(\beta g\theta_0)^2t$. Spatial-temporal scaling of velocity and temperature fluctuations is therefore expected to follow

$$\delta_r v(t)\simeq\epsilon^{1/3}r^{1/3}\simeq(\beta g\theta_0)^{2/3}t^{1/3}r^{1/3}, \tag{5}$$

$$\delta_r T(t)\simeq\epsilon^{-1/6}\epsilon_T^{1/2}r^{1/3}\simeq\theta_0^{2/3}(\beta g)^{-1/3}t^{-2/3}r^{1/3}, \tag{6}$$

where $\delta_r v(t)=v(x+r,t)-v(x,t)$ is the velocity increment on a separation r (similarly for temperature) and $\epsilon_T\simeq\theta_0^2t^{-1}$ is the temperature-variance flux. We remark that the above scaling is consistent with the assumption of the theory that temperature fluctuations are passively transported at small scales [indeed using Eqs. (5) and (6), the buoyancy term βgT becomes subleading in Eq. (1) at small scales]. This is the main difference with respect to the two-dimensional (2D) case in which temperature fluctuations force the turbulent flow at all scales.[4,7,22]

III. NUMERICAL SETTING

The Boussinesq equations (1) and (2) are integrated by a standard 2/3-dealiased pseudospectral method on a 3D periodic domain of square basis $L_x=L_y$ and aspect ratio $L_x/L_z=R$ with uniform grid spacing at different resolutions, as shown in Table I. In the following, all physical quantities are made dimensionless using the vertical scale L_z, the temperature jump θ_0, and the characteristic time $\tau=(L_z/Ag)^{1/2}$ as fundamental units.

Time evolution is obtained by a second-order Runge–Kutta scheme with explicit linear part. In all the runs, $\beta g=2.0$ and $\mathrm{Pr}=\nu/\kappa=1$. Viscosity is sufficiently large to resolve small scales ($k_{\rm max}\eta\simeq 1.2$ at final time, being $\eta=\nu^{3/4}\epsilon^{-1/4}$ the Kolmogorov scale and $k_{\rm max}=N_x/3$).

RT instability is seeded by perturbing the initial condition with respect to the unstable step profile. Two different perturbations were implemented in order to check the independence of the turbulent state from initial conditions. In the first case the interface $T=0$ at $z=0$ is perturbed by a superposition of 2D waves of small amplitude $h_0=0.004L_z$ in an isotropic range of wavenumbers $32\le k\le 64$ (with $k^2=k_x^2$

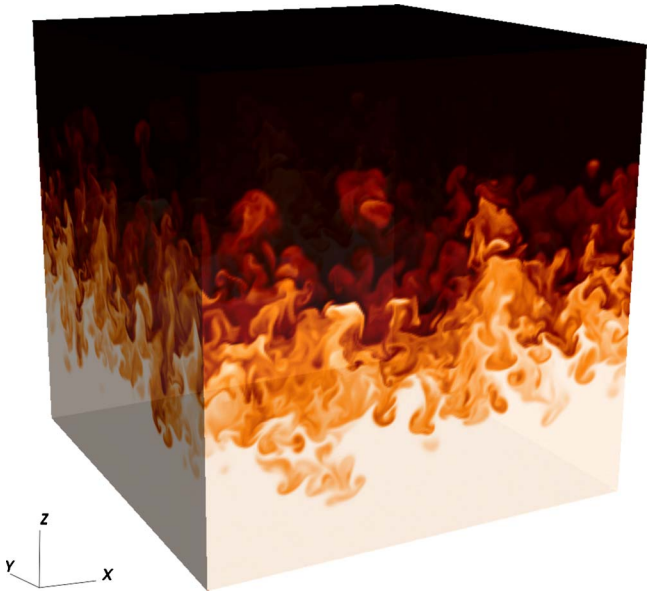

FIG. 1. (Color online) Snapshot of temperature field for the RT simulation at $t=2\tau$. White (black) regions correspond to hot (cold) fluid. Parameters in Table I, run B.

$+k_y^2$) and random phases.[23] For the second set of simulations, we perturbed the initial condition by adding 10% of white noise to the value of $T(\mathbf{x},0)$ in a layer of width h_0 around $z=0$. Figure 1 shows a snapshot of the temperature field in a cubic slice around $z=0$ in the turbulent regime at time $t=2\tau$ for simulation B (see Table I).

IV. EVOLUTION OF GLOBAL QUANTITIES

Figure 2 displays the evolution of the total kinetic energy $E=\int(1/2)v(\mathbf{x})^2 d\mathbf{x}$ and total kinetic-energy dissipation ϵ_L as a function of time. After the linear instability regime, at $t\simeq\tau$ the turbulent regime sets in with algebraic time dependence. Temporal evolution of the two quantities are easily obtained recalling that, being global quantities, an additional geometrical factor $h(t)\sim t^2$ due to the integration over the vertical direction has to be included. Therefore the predictions are

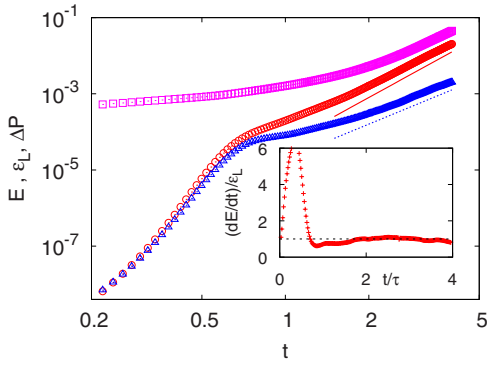

FIG. 2. (Color online) Temporal growth of kinetic energy E (circles), kinetic-energy dissipation ϵ_L (triangles), and potential-energy loss ΔP (squares) for run B. For clarity of the plot ϵ_L has been shifted by a factor 10. The two short lines represent the dimensional scaling $E(t)\sim\Delta P(t)\sim t^4$ and $\epsilon_L(t)\sim t^3$. Inset: ratio of the energy growth rate dE/dt and the flux ϵ_L. Data from run B.

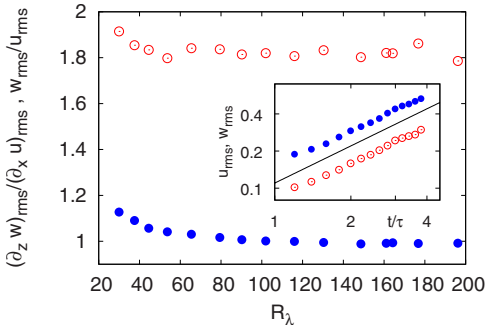

FIG. 3. (Color online) Ratio of the vertical rms velocity $w_{\rm rms}$ to the horizontal rms velocity $u_{\rm rms}$ (open circles) and ratio of the vertical velocity gradient $(\partial_z w)_{\rm rms}$ to the horizontal velocity gradient $(\partial_x u)_{\rm rms}$ (filled circles) vs Reynolds number R_λ indicating the recovery of isotropy at small scales. Inset: temporal evolution of horizontal rms velocity $u_{\rm rms}$ (open circles) and vertical rms velocity $w_{\rm rms}$ (filled circles). The line represents linear scaling. Data from run B.

$E(t)\sim v_{\rm rms}^2 h\sim t^4$ and $\epsilon_L\sim\epsilon h\sim t^3$, as indeed observed at late times. We also plot in Fig. 2 the total potential-energy loss, defined as $P(0)-P(t)$ with $P(t)=-\beta g\int zT(\mathbf{x})d\mathbf{x}$, which has the same temporal scaling of $E(t)$ as it is obvious from energy balance: $d(E+P)/dt=-\epsilon_L$. Notice that for this nonstationary turbulence the energy balance does not fix the ratio between the energy growth rate dE/dt and the energy dissipation (and flux) ϵ_L. In the turbulent regime, our simulations show an "equipartition" between large-scale energy growth and small-scale energy dissipation: $dE/dt\simeq\epsilon_L\simeq-(1/2)dP/dt$. This amounts to saying that half of the power injected into the flow contributes to the growth of the large-scale flow, and half feeds the turbulent cascade (see inset of Fig. 2). This result was found to be independent on the value of viscosity (the only adjustable parameter in the system) and is consistent with previous findings.[24]

An interesting remark is that RT turbulence represents an instance of the general case of a turbulent flow adiabatically evolving under a time-dependent energy input density $\mathcal{I}(t)$, which forces the flow at the integral scale $L(t)$ (concerning the problem of turbulent flow characterized by a time-dependent forcing, see, for example, Refs. 25 and 26 and references therein). Energy balance requires $d\mathcal{E}/dt=\mathcal{I}(t)-\epsilon(t)$, where $\mathcal{E}$ is the kinetic-energy density. Assuming a Kolmogorov spectrum for velocity fluctuations at scales smaller than the integral scale, one estimates $\mathcal{E}(t)\simeq\epsilon^{2/3}L^{2/3}$. Therefore, in situations characterized by an algebraic growth of the energy input density $\mathcal{I}(t)\sim t^\gamma$ a self-similar evolution of the energy spectrum can be obtained only if $\epsilon(t)\sim t^\gamma$ and $L(t)\sim t^{(3+\gamma)/2}$. This is indeed realized in RT turbulence, where $\gamma=1$ and $\epsilon\sim t$, $L(t)\sim t^2$.

In the inset of Fig. 3 the growth of vertical and horizontal rms velocity ($w_{\rm rms}$ and $u_{\rm rms}$, respectively), computed within the mixing layer, is shown. Both $u_{\rm rms}$ and $w_{\rm rms}$ grow linearly in time, as expected, with the vertical velocity about twice the horizontal one, reflecting the anisotropy of the forcing due to gravity. It is interesting to observe that anisotropy decays at small scales, where almost complete isotropy is recovered, as shown in Fig. 3. The ratio of vertical to horizontal rms velocity reaches a value of $w_{\rm rms}/u_{\rm rms}\simeq 1.8$ at

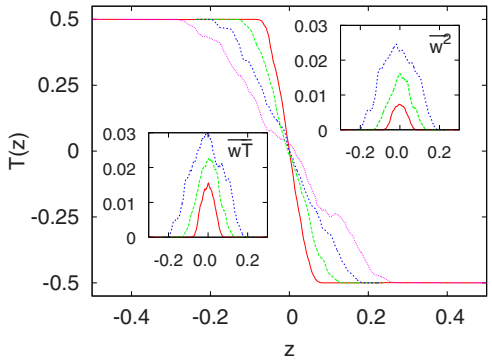

FIG. 4. (Color online) Mean temperature profiles $\bar{T}(z,t)$ for a single realization of simulation B with diffused initial perturbation at times $t=1.4\tau$, $t=2.0\tau$, $t=2.6\tau$, and $t=3.2\tau$. Lower and upper insets: profiles of the heat flux $\overline{wT}(z,t)$ and square vertical velocity $\overline{w^2}(z,t)$ at times $t=1.4\tau$, $t=2.0\tau$, and $t=2.6\tau$.

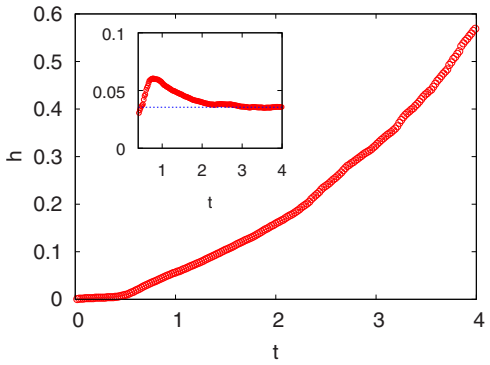

FIG. 5. (Color online) Evolution of the mixing layer width h as a function of time t for simulation B computed from the profiles of Fig. 4 with a threshold $s=0.8$. The inset shows the compensation with dimensional prediction $h/(Agt^2)$ converging to a value $\simeq 0.036$.

later times (corresponding to $R_\lambda \simeq 200$) while for the gradients we have $(\partial_z w)_{\rm rms}/(\partial_x u)_{\rm rms} \simeq 1.0$.

The evolution of the mean temperature profile $\bar{T}(z,t) \equiv 1/(L_x L_y)\int T(\mathbf{x},t)dxdy$ is shown in Fig. 4. As observed in previous simulations[10,11,22,27] the mean profile is approximately linear within the mixing layer (where therefore the system recovers statistical homogeneity). Nevertheless, statistical fluctuations of temperature in the mixing layer are relatively strong: At later time we find a flat profile of fluctuations. Moreover their distribution is close to a Gaussian with a standard deviation $\sigma_T(z) \simeq 0.25\theta_0$ (not shown here).

In Fig. 4 we also plot the profile of the heat flux $\overline{wT}(z,t)$ and the square vertical velocity $\overline{w^2}(z,t)$. Both vanish outside the mixing layer and inside show a similar shape not far from a parabola. Of course, the time behaviors of the heat flux and of the square vertical velocity amplitude are different. Indeed, the former is expected to grow as $\propto t$ and the latter as $\propto t^2$.

The mean temperature profile defines the width of the mixing layer. Different definitions of the mixing width, h, have been proposed on the basis of integral quantities or threshold values (see Ref. 28 for a discussion of the different methods). In the following we will use the simple definition based on a threshold value: $\bar{T}(\pm h/2)=s\theta_0/2$, where $s<1$ represents the threshold.

The evolution of the mixing width for $s=0.8$ is shown in Fig. 5. After an initial stage ($t<0.3\tau$) in which the perturbation relaxes toward the most unstable direction, we observe a short exponential growth corresponding to the linear RT instability. At later times ($t>0.6\tau$) the similarity regime sets in and the dimensional t^2 law is observed. The naive compensation with Agt^2 gives an asymptotic constant value of $h/(Agt^2) \simeq 0.036$ for $t \geq 3\tau$ and $\mathrm{Re} \simeq 10^4$ (at which the mixing width is still below half box). For the calculation of α, more sophisticated analysis have been proposed recently[3,29,30] using slightly different approaches (briefly, in Ref. 29 a similarity assumption and in Ref. 30 a mass flux and energy balance argument). In both cases, the authors derive for the evolution of $h(t)$ the equation

$$\dot{h}^2 = 4\alpha A g h, \tag{7}$$

which has solution $h(t)=\alpha A g t^2 + 2(\alpha A h_0)^{1/2} t + h_0$, where h_0 is the initial width introduced by the perturbation. $\alpha=\dot{h}^2/(4Agh)$. The idea is to get rid of the subleading terms and extract the t^2 contribution at early time by using directly Eq. (7) and evaluating $\alpha=\dot{h}^2/(4Agh)$.

The growth of the mixing layer width $h(t)$, a geometrical quantity, is accompanied by the growth of the integral scale $L(t)$, a dynamical quantity representing the typical size of the large-scale turbulent eddies. Following Ref. 9 we define L as the half width of the velocity correlation function $f(L)=\langle v_i(r)v_i(r+L)\rangle/\langle v^2\rangle = 1/2$. In the turbulent regime the integral scale and the mixing length are linearly related (see Fig. 6). A linear fit gives $L/h \simeq 1/17$ and $L/h \simeq 1/42$ for the integral scale based on the vertical and horizontal velocity components, respectively, in agreement with the results shown in Ref. 9 (of course, the precise values of the coefficients depend on the definition of h). The anisotropy of the large-scale flow is reflected in the velocity correlation length: The integral scale based on horizontal velocity is smaller than the one based on vertical velocity.

We end this section by discussing the behavior of the turbulent heat flux, the energy transfer, and the mean temperature gradient in terms of dimensionless variables (as dis-

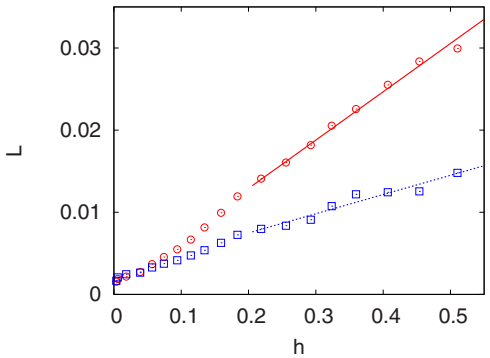

FIG. 6. (Color online) Growth of the integral scale L based on the vertical velocity (circles) and horizontal velocities (squares) as a function of the mixing layer h. Data from simulation B.

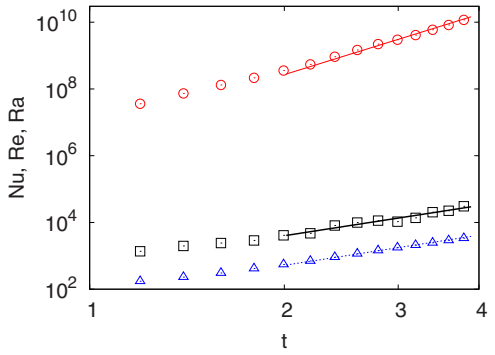

FIG. 7. (Color online) Temporal scaling of Nusselt number $\mathrm{Nu}=1+\langle wT\rangle h/(\kappa\theta_0)$ (triangles), Reynolds number $\mathrm{Re}=v_{\mathrm{rms}}h/\nu$ (squares), and Rayleigh number $\mathrm{Ra}=\beta g\theta_0 h^3/(\nu\kappa)$ (circles) for simulation *B* at Pr=1. The lines are the temporal scaling predictions t^3 for Nu and Re and t^6 for Ra.

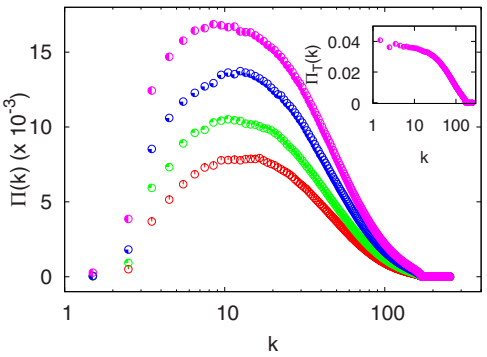

FIG. 9. (Color online) Spectral global kinetic-energy flux $\Pi(k)$ at times $t=2.4\tau$, $t=2.6\tau$, $t=2.8\tau$, and $t=3.0\tau$ (from bottom to top) and temperature-variance flux at $t=3.0\tau$ (inset) for simulation B. Kinetic-energy flux is defined as $\Pi(k)=-\int_k^\infty \mathrm{Re}[\hat{v}_i(-\mathbf{k}')\widehat{(\mathbf{v}\cdot\nabla\mathbf{v}_i)}(\mathbf{k}')]d\mathbf{k}'$, where $\hat{}$ is the Fourier transform (Ref. 8). A similar definition holds for the temperature-variance flux.

cussed in Sec II): Nusselt, Reynolds, and Rayleigh numbers, respectively. The temporal evolution of these numbers, shown in Fig. 7, follows the dimensional prediction (3) for the temporal evolution of α (see the inset in Fig. 5). The presence of the ultimate state of thermal convection, in the restricted case Pr=1, is also confirmed by our numerical results. Data obtained from simulations at various resolutions (see Fig. 8) are in close agreement with the "ultimate state" scaling (4).

V. SMALL-SCALE STATISTICS

As already discussed in Sec. I, the phenomenological theory predicts that at small scales, RT turbulence realizes an adiabatically evolving Kolmogorov–Obukhov scenario of NS turbulence. Here adiabatic means that because of the scaling laws, small scales have sufficient time to adapt to the variations of large scales, leading to a scale-independent energy flux. We remark that this is not the only possibility, as in two dimensions the phenomenology is substantially different. Unlike the 3D configuration, the 2D scenario is an example of active scalar problem. Indeed, the buoyancy effect is leading at both large and smaller scales. An adiabatic generalization of Bolgiano–Obukhov scaling has been predicted by means of mean-field theory[7] and has been confirmed numerically.[22]

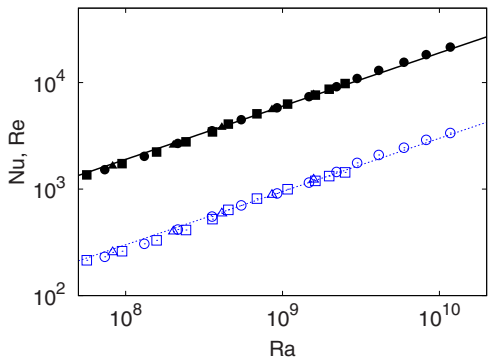

FIG. 8. (Color online) Nusselt (open symbols) and Reynolds (filled symbols) numbers as a function of Rayleigh number at Pr=1. The ultimate state prediction (lines) expressed by Eq. (4) is compared to numerical data obtained from simulations A (squares), B (circles), and C (triangles).

Figure 9 shows the global energy flux in spectral space at different times in the turbulent stage of the simulation. As discussed above, the flux grows in time following the increase in the input $\mathcal{I}(t)$ at large scales and at smaller ones, faster scales have time to adjust their intensities to generate a scale-independent flux.

If the analogy with NS turbulence is taken seriously, one can extend the dimensional predictions (5) and (6) to include intermittency effects. Structure functions for velocity and temperature fluctuations are therefore expected to follow

$$S_p(r,t)\equiv\langle(\delta_r v_\parallel(t))^p\rangle\simeq v_{\mathrm{rms}}(t)^p\left(\frac{r}{h(t)}\right)^{\zeta_p}, \tag{8}$$

$$S_p^T(r,t)\equiv\langle(\delta_r\theta(t))^p\rangle\simeq\theta_0^p\left(\frac{r}{h(t)}\right)^{\zeta_p^T}. \tag{9}$$

In Eq. (8) we introduce the longitudinal velocity differences $\delta_r v_\parallel(t)\equiv[\mathbf{v}(\mathbf{x}+\mathbf{r},t)-\mathbf{v}(\mathbf{x},t)]\cdot\mathbf{r}/r$ and the increment r is made dimensionless with a characteristic large scale which, in the present setup, is proportional to the width of the mixing layer $h(t)$, the only scale present in the system. The two sets of scaling exponents ζ_p and ζ_p^T are known from both experiments[31,32] and numerical simulations[33] with good accuracy for moderate p. Mean-field prediction is $\zeta_p=\zeta_p^T=p/3$ while intermittency leads to a deviation with respect to this linear behavior. Kolmogorov's "4/5" law for third-order velocity implies the exact result $\zeta_3=1$, while temperature exponents are not fixed, apart for standard inequality requirements.[8] Both experiments and simulations give stronger intermittency in temperature than in velocity fluctuations, i.e., $\zeta_p^T<\zeta_p$ for large p.

We have computed velocity and temperature structure functions and spectra in our simulations of RT turbulence. To overcome the inhomogeneity of the setup, velocity and temperature differences (at fixed time) are taken between points both belonging to the mixing layer as defined above. Isotropy is recovered by averaging the separation $\mathbf{r}$ over all directions. Spectra are computed by the Fourier-transforming velocity and temperature fields on 2D horizontal planes and then averaging vertically over the mixing layer.

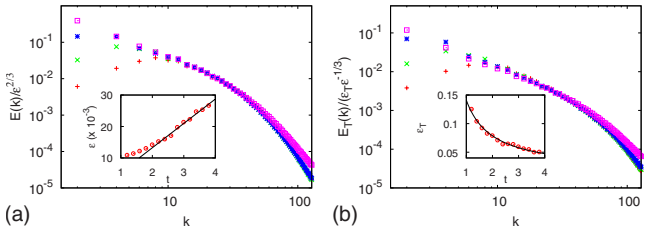

FIG. 10. (Color online) (a) Kinetic-energy spectra compensated with $\epsilon^{2/3}$ at times $t=1\tau$ (crosses), $t=1.4\tau$ (times), $t=1.8\tau$ (stars), and $t=3.8\tau$ (squares). Inset: kinetic-energy dissipation vs time. The line represents the linear growing of energy dissipation (see Sec. II). (b) Temperature-variance spectra compensated with $\epsilon_T^{-1}\epsilon^{1/3}$ at same times. Inset: temperature-variance dissipation vs time. The line is the dimensional prediction $\sim t^{-1}$ (see Sec. II). Data from simulation B.

A. Lower-order statistics

In Fig. 10(a), we plot kinetic-energy spectra at different times in the turbulent stage, compensated with the time-dependent energy dissipation $\epsilon^{2/3}(t)$. In the intermediate range of wavenumbers, corresponding to inertial scales, the collapse is almost perfect. The evolution of the compensated spectra shows that the growth of the integral scale at small wavenumbers is in agreement with Fig. 6. Likewise temperature-variance spectra are considered in Fig. 10(b). Here, the spectra are compensated with both the time-dependent temperature-variance dissipation $\epsilon_T^{-1}(t)$ and the energy dissipation $\epsilon^{1/3}(t)$. The evolution of the intermediate range of wavenumbers follows the dimensional prediction (6).

Figure 11 displays the third-order velocity structure function $S_3(r)$, related to the energy flux by Kolmogorov's 4/5 law $S_3(r)=-(4/5)\epsilon r$.[8] We also plot the mixed velocity-temperature structure function $S_{1,2}(r)\equiv\langle\delta_r v_\parallel(\delta_r T)^2\rangle$, which is proportional to the (constant) flux of temperature fluctuations ϵ_T according to Yaglom's law $S_{1,2}(r)=-(4/3)\epsilon_T r$.[34] Both the computed structure functions display a range of linear scaling, i.e., a constant flux, in the inertial range of scales $5\times10^{-3}\leq r/L_z\leq5\times10^{-2}$. It is interesting to observe that the mixed structure function $S_{1,2}(r)$ seems to have a range of scaling which extends to larger scales. This is probably due

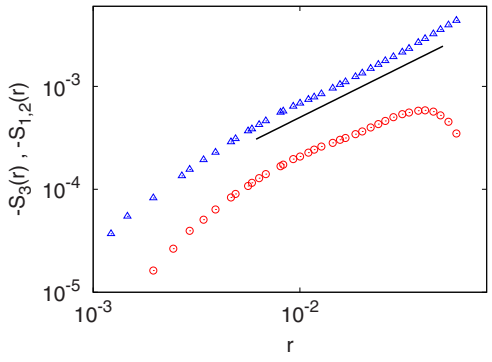

FIG. 11. (Color online) Third-order isotropic longitudinal velocity structure function $S_3(r)$ computed at a late stage in the simulation (circles) and mixed longitudinal velocity-temperature structure function $S_{1,2}(r)$ (triangles). The black line represents the linear scaling. Data from simulation B.

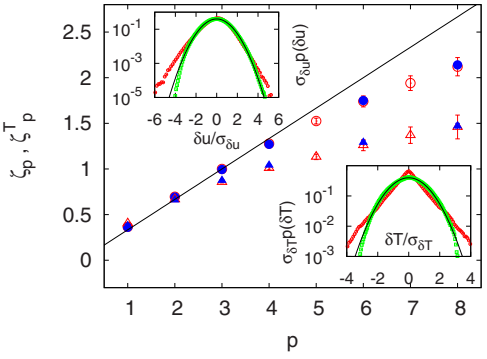

FIG. 12. (Color online) Structure-function scaling exponents for velocity increments ζ_p (circles) and temperature increments ζ_p^T (triangles) with absolute values. Red open symbols are obtained using ESS procedure (Ref. 35) on the present simulation at time $t=3\tau$, fixing the values of $\zeta_3=1$ and $\zeta_2^T=2/3$. Errors represent fluctuations observed in different realizations of simulation B. Blue filled symbols are taken from a stationary NS simulation at $R_\lambda=427$ (Ref. 33). Black line is Kolmogorov nonintermittent scaling $p/3$. Insets: probability density function for velocity differences $\delta_r v(t)$ (upper) and temperature differences $\delta_r T(t)$ at time $t=3\tau$ and scales $r=0.008L_z$ (circles) and $r=0.06L_z$ (squares). Black lines represent a standard Gaussian.

to the fact that at large-scale temperature fluctuations are dominated by unmixed plumes which have strong correlations with vertical velocity.

B. Spatial/temporal intermittency

Despite the clear scaling observable in Fig. 11, it is very difficult to compute scaling exponents directly from higher-order structure functions because of limited Reynolds number and statistics. Therefore, assuming a scaling region as in Fig. 11, we can compute *relative* scaling exponents using the so-called extended self-similarity (ESS) procedure.[35] This corresponds to consider the scaling of one structure function with respect to a reference one [e.g., $S_3(r)$ for velocity statistics], and thus to measure a relative exponent (i.e., ζ_p/ζ_3).

Scaling exponents obtained in this way are shown in Fig. 12. Reference exponents for the ESS procedure are $\zeta_3=1$ and $\zeta_2^T=2/3$ (which is not an exact result). We see that both velocity and temperature scaling exponents deviate from the dimensional prediction of Eqs. (5) and (6) (i.e., $\zeta_p=\zeta_p^T=p/3$) indicating intermittency in the inertial range. We also observe a stronger deviation for temperature exponents, which is consistent with what is known for the statistics of a passive scalar advected by a turbulent flow.[8,36]

The question regarding the universality of the set of scaling exponents with respect to the geometry and the large-scale forcing naturally arises. Several experimental and numerical investigations in 3D turbulence support the universality scenario in which the set of velocity and passive scalar scaling exponents are independent of the details of large-scale energy injection and geometry of the flow. Therefore, because we have seen that in 3D RT turbulence at small scales temperature becomes passively transported and isotropy is recovered, one is tempted to compare scaling exponents with those obtained in NS turbulence. As shown in Fig. 12, the two sets of exponents coincide, within the error bars, with the exponents obtained from a standard NS simulation with passive scalar at comparable R_λ.[33]

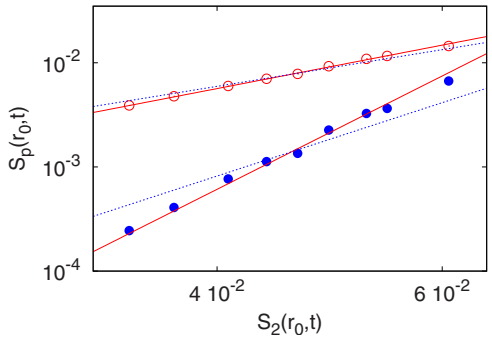

FIG. 13. (Color online) Time dependence of p-order velocity structure function $S_p(r_0,t)$ vs $S_2(r_0,t)$ for $p=4$ (red open circles) and $p=8$ (blue filled circles) with $r_0/L_z=0.012$, in the middle of the inertial range for simulation B. Red, continuous lines represent the intermittent prediction $\beta_p=p-2\zeta_p$ with ζ_p given by spatial structure functions; blue dashed lines are the nonintermittent prediction $\beta_p=p/3$.

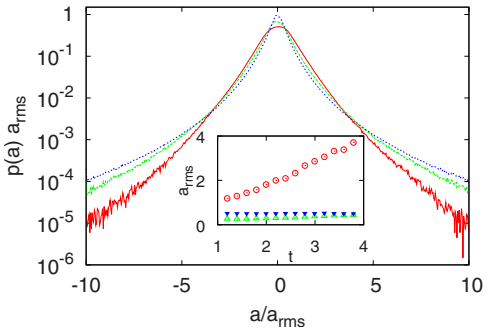

FIG. 14. (Color online) Probability density function of the vertical component of the acceleration at time $t=1\tau$ (red, bottom tails), $t=2\tau$ (green, intermediate tails), and $t=3.8\tau$ (blue, upper tails) normalized with rms values. Inset: evolution of $a_{\rm rms}$ with time for the three contributions of Eq. (1): pressure gradient $\partial_z p$ (red circles), dissipation $\nu\Delta w$ (green open triangles), and buoyancy term βgT (blue filled triangles). Data from simulation B.

We remark that scaling exponents for passive scalar in NS turbulence are very sensitive to the fitting procedure. Strong temporal fluctuations have been observed in single realization[37] and dependence on the fitting region has been reported.[33] Indeed, different realizations of RT turbulence (starting with slightly different initial perturbations) lead to fluctuations of scaling exponents which account for the error bars shown in Fig. 12.

Figure 12 also shows probability density functions for velocity and temperature fluctuations for two different scales. Both distributions are close to a Gaussian at large scale and develop wide tails at small scales, indicating the absence of self-similarity thus confirming the intermittency scenario.

As a further numerical support of Eqs. (8) and (9) we now consider temporal behavior of structure functions. From Eq. (8), taking into account the temporal evolution of large-scale quantities, we expect the temporal scaling $S_p(t)\sim t^{\beta_p}$ with $\beta_p=p-2\zeta_p$. With the Kolmogorov scaling one simply has $\beta_p=p/3$ but intermittent corrections are expected to be important, for example, $\beta_6\simeq 2.4$ instead of $p/3=2$. Figure 13 shows the scaling of $S_p(r,t)$ versus $S_2(r,t)$ (i.e., in the ESS framework) for a particular value of $r=r_0=0.0012L_z$. The relative temporal exponents β_p/β_2 obtained from the spatial exponents ζ_p of Fig. 12 fit well the data, while nonintermittent relative scaling exponents $\beta_p/\beta_2=p/2$ are ruled out.

The effects of intermittency are particularly important at very small scales. One important example is the statistics of acceleration which has recently been the object of experimental and numerical investigations.[38,39] For completeness, we briefly recall the main results obtained in those studies.

The acceleration a of a Lagrangian particle transported by the turbulent flow is by definition given by the right hand side of Eq. (1). In the present case of the Boussinesq approximation, the acceleration has three contributions: pressure gradient, viscous dissipation, and buoyancy terms. Neglecting intermittency for the moment, dimensional scalings (5) and (6), implies that $-\nabla p\simeq \nu\triangle u\simeq \nu^{-1/4}(\beta g\theta_0)^{3/2}t^{3/4}$ while $\beta gT\simeq\beta g\theta_0$. Therefore the buoyancy term in Eq. (1) becomes subleading not only going to small scales but also at later times. Among the other two terms, we find that as in standard NS turbulence, the pressure gradient term is by far the dominant one, as shown in the inset of Fig. 14. After an initial transient, we have that for $t\geq 2\tau$ both terms grow with a constant ratio $(\partial_z p)_{\rm rms}/(\nu\triangle w)_{\rm rms}\simeq 8$.

The inset of Fig. 14 suggests that the temporal growth of $a_{\rm rms}$ is faster than $t^{3/4}$. Again, this can be understood as an effect of intermittency which is particularly important at small scales. Indeed, using the multifractal model of intermittency[8] one obtains the prediction $a_{\rm rms}\sim t^{0.86}$.[39]

The effect of intermittency on acceleration statistics is evident by looking at the probability density function (pdf). Figure 14 shows that the distribution develops larger tails as turbulence intensity, and Reynolds number, increases. This effect is indeed expected, as the shape of the acceleration pdf depends on the Reynolds number and therefore no universal form is reached. Nevertheless, given the value of R_λ as a parameter, the pdf can be predicted again using the multifractal model.[39]

VI. CONCLUSION

We have studied spatial and temporal statistics of RT turbulence in three dimensions at small Atwood number and at Prandtl number one on the basis of a set of high resolution numerical simulations. RT turbulence is a paradigmatic example of nonstationary turbulence with a time-dependent injection scale. The phenomenological theory proposed by Chertkov[7] is based on the notion of adiabaticity where small scales are slaved to large ones: The latter are forced by conversion of potential energy into kinetic energy and the former undergo a turbulence cascade flowing to smaller scales until molecular viscosity becomes important. In this picture, temperature actively forces hydrodynamic degrees of freedom at large scales while it behaves like a passive scalar field at small scales where a constant kinetic-energy flux develops.

The above scenario suggests comparison of RT turbulence with classical homogeneous, isotropic, and stationary NS turbulence, in the general framework of the existence of universality classes in turbulence.

By means of accurate direct numerical simulations, we provide numerical evidence in favor of the mean-field theory. Moreover, we extend the analysis to higher-order statistics thus addressing the issue related to intermittency corrections.

By measuring scaling exponents of both velocity and temperature structure functions, we find that indeed they are compatible with those obtained in standard turbulence. This result gives further support for the universality scenario.

We also investigate temporal evolution of global quantities, both geometrical (the width of mixing layer) and dynamical (the heat flux). The relevant dimensionless quantities in RT turbulence are the Rayleigh, Reynolds, and Nusselt numbers for which there exists an old prediction due to Kraichnan,[19] known as the ultimate state of thermal convection, which links the dimensionless number in terms of simple scaling laws. Our set of numerical simulations give again strong evidence for the validity of such scaling in RT turbulence at small Atwood number and at Prandtl number one thus confirming how important in thermal convection is the role of boundaries, which prevent the emergence of the ultimate state.

[1] L. Rayleigh, "Analytic solutions of the Rayleigh equation for linear density profiles," Proc. London Math. Soc. **14**, 170 (1883).
[2] G. Taylor, "The instability of liquid surfaces when accelerated in a direction perpendicular to their planes," Proc. R. Soc. London **201**, 192 (1950).
[3] W. H. Cabot and A. W. Cook, "Reynolds number effects on Rayleigh–Taylor instability with possible implications for type Ia supernovae," Nat. Phys. **2**, 562 (2006).
[4] M. Zingale, S. E. Woosley, J. B. Bell, M. S. Day, and C. A. Rendleman, "The physics of flames in type Ia supernovae," Astrophys. J. **632**, 1021 (2005).
[5] S. P. Regan, J. A. Delettrez, F. J. Marshall, J. M. Soures, V. A. Smalyuk, B. Yaakobi, R. Epstein, V. Yu. Glebov, P. A. Jaanimagi, D. D. Meyerhofer, P. B. Radha, T. C. Sangster, W. Seka, S. Skupsky, C. Stoeckl, and R. P. J. Town, "Shell mix in the compressed core of spherical implosions," Phys. Rev. Lett. **89**, 085003 (2002).
[6] S. Fujioka, A. Sunahara, K. Nishihara, N. Ohnishi, T. Johzaki, H. Shiraga, K. Shigemori, M. Nakai, T. Ikegawa, M. Murakami, K. Nagai, T. Norimatsu, H. Azechi, and T. Yamanaka, "Suppression of the Rayleigh–Taylor instability due to self-radiation in a multiablation target," Phys. Rev. Lett. **92**, 195001 (2004).
[7] M. Chertkov, "Phenomenology of Rayleigh–Taylor turbulence," Phys. Rev. Lett. **91**, 115001 (2003).
[8] U. Frisch, *Turbulence: The Legacy of A. N. Kolmogorov* (Cambridge University Press, Cambridge, 1995).
[9] N. Vladimirova and M. Chertkov, "Self-similarity and universality in Rayleigh–Taylor, Boussinesq turbulence," Phys. Fluids **21**, 015102 (2009).
[10] T. Matsumoto, "Anomalous scaling of three-dimensional Rayleigh–Taylor turbulence," Phys. Rev. E **79**, 055301 (2009).
[11] G. Boffetta, A. Mazzino, S. Musacchio, and L. Vozella, "Kolmogorov scaling and intermittency in Rayleigh–Taylor turbulence," Phys. Rev. E **79**, 065301 (2009).
[12] Y. Zhou, "A scaling analysis of turbulent flows driven by Rayleigh–Taylor and Richtmyer–Meshkov instabilities," Phys. Fluids **13**, 538 (2001).
[13] E. D. Siggia, "High Rayleigh number convection," Annu. Rev. Fluid Mech. **26**, 137 (1994).
[14] J. A. Glazier, T. Segawa, A. Naert, and M. Sano, "Evidence against 'ultrahard' thermal turbulence at very high Rayleigh numbers," Nature (London) **398**, 307 (1999).
[15] J. J. Niemela, L. Skrbek, K. R. Sreenivasan, and R. J. Donnelly, "Turbulent convection at very high Rayleigh numbers," Nature (London) **404**, 837 (2000).
[16] X. Xu, K. M. S. Bajaj, and G. Ahlers, "Heat transport in turbulent Rayleigh–Bénard convection," Phys. Rev. Lett. **84**, 4357 (2000).
[17] A. Nikolaenko and G. Ahlers, "Nusselt number measurements for turbulent Rayleigh–Bénard convection," Phys. Rev. Lett. **91**, 084501 (2003).
[18] S. Grossmann and D. Lohse, "Scaling in thermal convection: A unifying theory," J. Fluid Mech. **407**, 27 (2000).
[19] R. H. Kraichnan, "Turbulent thermal convection at arbitrary Prandtl number," Phys. Fluids **5**, 1374 (1962).
[20] C. R. Doering and P. Constantin, "Variational bounds on energy dissipation in incompressible flows. III. Convection," Phys. Rev. E **53**, 5957 (1996).
[21] D. Lohse and F. Toschi, "Ultimate state of thermal convection," Phys. Rev. Lett. **90**, 034502 (2003).
[22] A. Celani, A. Mazzino, and L. Vozella, "Rayleigh–Taylor turbulence in two dimensions," Phys. Rev. Lett. **96**, 134504 (2006).
[23] P. Ramaprabhu, G. Dimonte, and M. Andrews, "A numerical study of the influence of initial perturbations on the turbulent Rayleigh–Taylor instability," J. Fluid Mech. **536**, 285 (2005).
[24] P. Ramaprabhu and M. Andrews, "Experimental investigation of Rayleigh–Taylor mixing at small Atwood numbers," J. Fluid Mech. **502**, 233 (2004).
[25] A. von der Heydt, S. Grossmann, and D. Lohse, "Response maxima in modulated turbulence," Phys. Rev. E **67**, 046308 (2003).
[26] A. K. Kuczaj, B. J. Geurts, D. Lohse, and W. van de Water, "Turbulence modification by periodically modulated scale-dependent forcing," Comput. Fluids **37**, 816 (2008).
[27] A. W. Cook and P. E. Dimotakis, "Transition stages of Rayleigh–Taylor instability between miscible fluids," J. Fluid Mech. **443**, 69 (2001).
[28] S. Dalziel, P. Linden, and D. Youngs, "Self-similarity and internal structure of turbulence induced by Rayleigh–Taylor instability," J. Fluid Mech. **399**, 1 (1999).
[29] J. Ristorcelli and T. Clark, "Rayleigh–Taylor turbulence: Self-similar analysis and direct numerical simulations," J. Fluid Mech. **507**, 213 (2004).
[30] A. W. Cook, W. H. Cabot, and P. L. Miller, "The mixing transition in Rayleigh–Taylor instability," J. Fluid Mech. **511**, 333 (2004).
[31] Z. Warhaft, "Passive scalar in turbulent flows," Annu. Rev. Fluid Mech. **32**, 203 (2000).
[32] F. Moisy, H. William, J. S. Andersen, and P. Tabeling, "Passive scalar intermittency in low temperature helium flows," Phys. Rev. Lett. **86**, 4827 (2001).
[33] T. Watanabe and T. Gotoh, "Statistics of a passive scalar in homogeneous turbulence," New J. Phys. **6**, 40 (2004).
[34] A. M. Yaglom, "On the local structure of a temperature field in a turbulent flow," Dokl. Akad. Nauk SSSR **69**, 743 (1949).
[35] R. Benzi, S. Ciliberto, R. Tripiccione, C. Baudet, F. Massaioli, and S. Succi, "Extended self-similarity in turbulent flows," Phys. Rev. E **48**, R29 (1993).
[36] K. R. Sreenivasan and R. A. Antonia, "The phenomenology of small-scale turbulence," Annu. Rev. Fluid Mech. **29**, 435 (1997).
[37] S. Chen and N. Chao, "Anomalous scaling and structure instability in three-dimensional passive scalar turbulence," Phys. Rev. Lett. **78**, 3459 (1997).
[38] A. La Porta, G. A. Voth, A. M. Crawford, J. Alexander, and E. Bodenschatz, "Fluid particle accelerations in fully developed turbulence," Nature (London) **409**, 1017 (2001).
[39] L. Biferale, G. Boffetta, A. Celani, B. J. Devenish, A. Lanotte, and F. Toschi, "Multifractal statistics of Lagrangian velocity and acceleration in turbulence," Phys. Rev. Lett. **93**, 064502 (2004).